are maintained. However, when *ddm1* is back-crossed to the wild type, hypomethylated DNA is epigenetically inherited in subsequent generations (*8*). Further, epimutant alleles at the *SUPERMAN* locus arise at elevated frequencies in *ddm1*, but they are overmethylated rather than undermethylated (*20*).

We can account for these observations if DNA methylation during replication depends on a high concentration of H3mK9 in a given chromosomal domain. According to this scenario, redistribution of methylated histones in *ddm1* would lead to dilution of heterochromatic H3mK9 relative to H3mK4 and to subsequent loss of DNA methylation. When *ddm1* is crossed back to the wild type, de novo DNA methylation of transposons would fail to occur, because histone methylation patterns could not be restored once they were lost (*12*). The aberrant association of H3mK9 with euchromatic sequences in *ddm1* could also lead to sporadic hypermethylation of euchromatic genes such as *SUPERMAN*, and even to retargeting of transposable elements to euchromatic sites if transposons themselves recognize H3mK9 (*21*).

Recently, it has been shown that DNA methylation in *Neurospora* depends on *dim5* (*22*), which encodes a homolog of mouse *Su(var)3-9* and fission yeast *clr4* (*12*). These are K9-specific histone H3 methyltransferases characterized by a specific SET [Su(var)3-9, Enhancer-of-zeste, Trithotrax] domain. *Arabidopsis* has up to 15 genes that potentially encode this class of proteins (*23*), and *KRYPTONITE* (*KYP-1*) resembles *dim5* in that it is also required for DNA methylation, affecting *SUPERMAN* and a number of retrotransposons (*24*). H3mK9-dependent DNA methylation is conferred by the methyltransferase CHROMOMETHYLASE3, which binds H3mK9 indirectly via an HP1-like protein. However, overall DNA methylation losses are modest in *kyp-1* relative to *ddm1*, presumably because of gene redundancy.

Together these results provide a mechanistic basis for the loss of DNA methylation in *ddm1*, as a consequence of the reduced association of heterochromatin with H3mK9. However, DNA methylation could also reinforce histone methylation patterns via chromatin-remodeling complexes that bind methylated DNA (*25*). The pattern of histone tail modification at specific amino acid residues has been proposed to represent a "histone code," established by modifying enzymes and interpreted by nucleosome-binding proteins (*12*). According to this model, DDM1 and other chromatin remodeling enzymes would "typeset" the code to ensure accurate compartmentalization of modified nucleosomes after replication. It remains to be seen whether DDM1 and other SWI/SNF subfamilies interact specifically with methylated and otherwise modified nucleosomes (*26*).

In an accompanying paper, Volpe *et al.* (*27*) show that H3mK9 can be targeted to heterochromatic repeats in the fission yeast *Schizosaccharomyces pombe* by RNA interference (RNAi). In *Caenorhabditis elegans* and *Drosophila*, which lack DNA methylation, transposons and repeats are also a target of RNAi (*28*, *29*). In organisms that have DNA methylation, H3mK9 is both interpreted by DNA methyltransferases (*22*, *24*) and reinforced by histone deacetylase complexes that bind methylated DNA (*25*). Further, induction of H3mK9 by noncoding RNA has been implied in mouse X-inactivation (*30*). Taken together, these results suggest a model whereby RNAi initiates transposon methylation by imposing H3mK9, which is then maintained through chromatin remodeling by DDM1. These mechanisms may account for the preferential methylation of transposons in plants and other eukaryotes (*21*).

References and Notes

1. C. Muchardt, M. Yaniv, *J. Mol. Biol.* **293**, 187 (1999).
2. G. Langst, P. B. Becker, *J. Cell Sci.* **114**, 2561 (2001).
3. A. Flaus, T. Owen-Hughes, *Curr. Opin. Genet. Dev.* **11**, 148 (2001).
4. M. L. Verbsky, E. J. Richards, *Curr. Opin. Plant Biol.* **4**, 494 (2001).
5. K. Dennis, T. Fan, T. Geiman, Q. Yan, K. Muegge, *Genes Dev.* **15**, 2940 (2001).
6. R. J. Gibbons *et al.*, *Nature Genet.* **24**, 368 (2000).
7. J. A. Jeddeloh, J. Bender, E. J. Richards, *Genes Dev.* **12**, 1714 (1998).
8. A. Vongs, T. Kakutani, R. A. Martienssen, E. J. Richards, *Science* **260**, 1926 (1993).
9. CSHL/WUGSC/PEB *Arabidopsis* Sequencing consortium, *Cell* **100**, 377 (2000).
10. T. L. Stokes, B. N. Kunkel, E. J. Richards, *Genes Dev.* **16**, 171 (2002).
11. J. A. Jeddeloh, T. L. Stokes, E. J. Richards, *Nature Genet.* **22**, 94 (1999).
12. T. Jenuwein, C. D. Allis, *Science* **293**, 1074 (2001).
13. P. F. Fransz *et al.*, *Cell* **100**, 367 (2000).
14. Information on materials and methods is available on *Science* Online.
15. Supplementary data are available on *Science* Online.
16. P. D. Rabinowicz *et al.*, *Nature Genet.* **23**, 305 (1999).
17. T. Singer, C. Yordan, R. A. Martienssen, *Genes Dev.* **15**, 591 (2001).
18. A. Miura *et al.*, *Nature* **411**, 212 (2001).
19. H. Hirochika, H. Okamoto, T. Kakutani, *Plant Cell* **12**, 357 (2000).
20. T. Kakutani, J. A. Jeddeloh, S. K. Flowers, K. Munakata, E. J. Richards, *Proc. Natl. Acad. Sci. U.S.A.* **93**, 12406 (1996).
21. R. A. Martienssen, V. Colot, *Science* **293**, 1070 (2001).
22. H. Tamaru, E. U. Selker, *Nature* **414**, 277 (2001).
23. L. O. Baumbusch *et al.*, *Nucleic Acids Res.* **29**, 4319 (2001).
24. J. P. Jackson, A. M. Lindroth, X. Cao, S. E. Jacobsen, *Nature* **416**, 556 (2002).
25. A. P. Bird, A. P. Wolffe, *Cell* **99**, 451 (1999).
26. P. Sudarsanam, F. Winston, *Trends Genet.* **16**, 345 (2000).
27. T. A. Volpe *et al.*, *Science* **297**, 1833 (2002).
28. R. F. Ketting, T. H. Haverkamp, H. G. van Luenen, R. H. Plasterk, *Cell* **99**, 133 (1999).
29. A. A. Aravin *et al.*, *Curr. Biol.* **11**, 1017 (2001).
30. E. Heard *et al.*, *Cell* **107**, 727 (2001).

31. We thank N. Dedhia for sequence analysis; J. Nakayama and M. Narita for advice on chromatin immunoprecipitation; and E. Richards, W. R. McCombie, and S. Grewal for helpful discussions. A.V.G. is supported by a graduate studentship from the French Ministry of Research. Z.L. is an Arnold and Mabel Beckman Anderson Fellow of the Watson School of Biological Sciences. This work was supported by a grant from NSF (NSF DBI-0077774).

Supporting Online Material

www.sciencemag.org/cgi/content/full/1074950/DC1
Materials and Methods
Table S1
References and Notes

11 June 2002; accepted 12 June 2002
Published online 20 June 2002;
10.1126/science.1074950
Include this information when citing this paper.

A Photoactivatable GFP for Selective Photolabeling of Proteins and Cells

George H. Patterson and Jennifer Lippincott-Schwartz*

We report a photoactivatable variant of the *Aequorea victoria* green fluorescent protein (GFP) that, after intense irradiation with 413-nanometer light, increases fluorescence 100 times when excited by 488-nanometer light and remains stable for days under aerobic conditions. These characteristics offer a new tool for exploring intracellular protein dynamics by tracking photoactivated molecules that are the only visible GFPs in the cell. Here, we use the photoactivatable GFP both as a free protein to measure protein diffusion across the nuclear envelope and as a chimera with a lysosomal membrane protein to demonstrate rapid interlysosomal membrane exchange.

Photoactivation, the rapid conversion of photoactivatable molecules to a fluorescent state by intense irradiation, can be used to mark and monitor selected molecules within cells (*1*). Previous efforts to develop a photoactivatable protein capable of high optical contrast when photoactivated under physiological conditions have had limited success (*2*–*5*). GFP's inherent brightness and suitability as a fusion protein in living cells (*6*, *7*) have prompted us to try to develop a variant that would allow selective marking of proteins through photoactivation.

Our efforts began with a codon-opti-

mized version of wild-type GFP [WEGFP; methods (*8*) supporting online text (*9*)]. Wild-type GFP normally exists as a mixed population of neutral phenols and anionic phenolates (Fig. 1A), which produces the major 397-nm and minor 475-nm absorbance peaks, respectively (Fig. 1B, filled circles) (*10*–*12*). Upon intense illumination of the protein with ultraviolet or ~400-nm light, the chromophore population undergoes photoconversion (*9*) and shifts predominantly to the anionic form (Fig. 1A), giving rise to an increase in minor peak absorbance (Fig. 1B, open squares). This produces an increase in fluorescence of about threefold upon excitation at 488 nm (*2*). We sought to develop a variant of WEGFP whose minor absorbance peak was initially lower, in the hope that photoconversion with ~400-nm irradiation would produce a greater increase in absorbance at the minor peak and thus a more noticeable optical contrast under 488-nm excitation.

A previously reported isoleucine mutation at the threonine 203 position (T203) of wild-type GFP reduces absorbance at 488 nm but maintains a normal major absorbance peak (*13*, *14*). We produced this and several other substitutions at the 203 position in an attempt to identify a mutant with minimized minor peak absorbance (table S1). Notable was the histidine substitution (i.e., T203H), which had barely detectable absorbance at the minor peak (Fig. 1C, filled circles) (*8*). To test the photoconversion properties of the T203H variant, we irradiated it with 413-nm laser light (*8*), which resulted in increased absorbance in the minor peak region (Fig. 1C, open squares). The fluorescence emission peak of the photoconverted T203H mutant was slightly red-shifted relative to WEGFP (Fig. 1D). Irradiation of several other T203 variants with 413-nm light revealed that they also underwent photoconversion, but none showed as large an increase in their minor absorbance peak as the T203H variant (table S1). These findings suggested that the T203H variant would serve well as a photoactivatable GFP. Therefore, we named it PA-GFP (for photo and activatable) and proceeded to study its properties further.

The degree of fluorescence enhancement under 488-nm excitation after photoactivation of PA-GFP, WEGFP, and the other T203 variants was determined in vitro on purified preparations of the protein embedded within polyacrylamide gels (*8*) (Fig. 2A; table S1). A fluorescence increase of ~100-fold for PA-GFP was observed (Fig. 2B). By contrast,

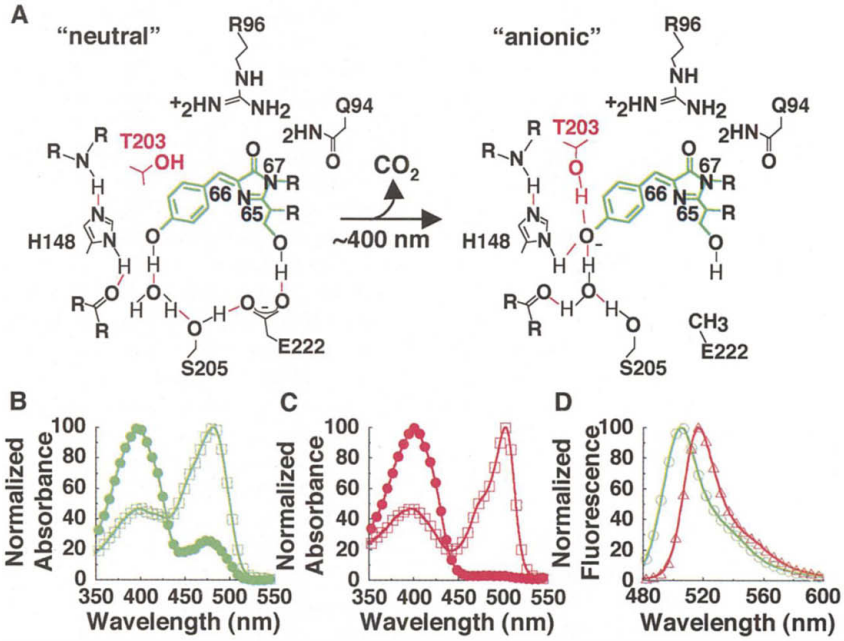

Fig. 1. Absorbance and emission spectra of photoactivated green fluorescent proteins. (**A**) Photoconversion in wild-type GFP is thought to involve a shift in the chromophore population from the neutral phenolic form to the anionic phenolate form. Rotation of the T203 and decarboxylation of glutamic acid 222 (E222) (*12*) are structural rearrangements that may be key features of GFP photoconversion (*9*). Native (filled circles) and photoactivated (open squares) absorbance spectra of (**B**) WEGFP (wild-type EGFP) and (**C**) T203H mutant (PA-GFP) are shown normalized to the highest absorbance. (**D**) Emission spectra were collected under excitation at 475 nm of photoactivated WEGFP (green circles) and PA-GFP (red triangles).

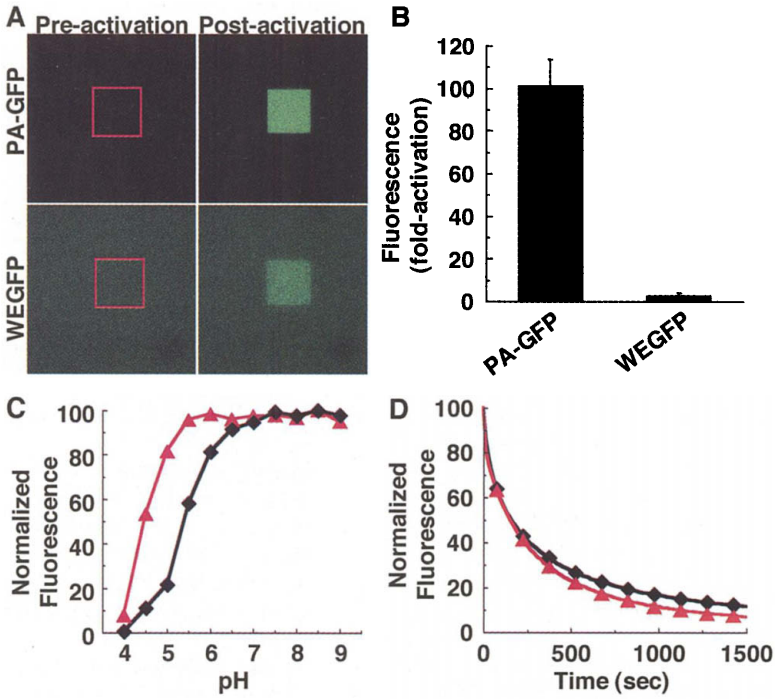

Fig. 2. Photoactivation and imaging in vitro. (**A**) Purified PA-GFP and WEGFP were embedded in 15% polyacrylamide beneath a coverslip and imaged by using low levels of 488-nm excitation before (preactivation) and after 413-nm irradiation (postactivation) within the regions indicated by the red squares. (**B**) Fluorescence increases under 488-nm excitation were determined by measuring the mean pixel values within the regions denoted by the red squares before and after photoactivation. (**C**) The level of fluorescence was determined from PA-GFP (red triangles) and EGFP (black diamonds) buffered at various pH levels (4.0 to 9.0). (**D**) Purified PA-GFP and EGFP were embedded in polyacrylamide to compare photobleaching of photoactivated PA-GFP (red triangles) with EGFP (black diamonds) under continuous high-intensity 488-nm irradiation.

Cell Biology and Metabolism Branch, National Institute of Child Health and Human Development, National Institutes of Health, Bethesda, MD 20892, USA.

*To whom correspondence should be addressed. E-mail: jlippin@helix.nih.gov

the other T203 variants showed significantly less optical contrast after photoactivation (table S1), and WEGFP showed an increase in fluorescence of only about threefold after photoactivation (Fig. 2, A and B).

PA-GFP displayed remarkable stability under a number of conditions. The photoactivated absorbance spectrum (Fig. 1C, open squares) was maintained for at least 1 week at 37°C. Its native fluorescence displayed more stability than EGFP fluorescence in the 5.5 to 9.0 pH range (Fig. 2C; fig. S1) and maintained ≥50-fold optical enhancement down to pH 5.0 (fig. S2). Repeated irradiation with high levels of 488-nm light (*8*) indicated that the photostability of photoactivated PA-GFP was comparable to EGFP (Fig. 2D).

We next investigated the photoactivation properties of PA-GFP when expressed in living cells. Before photoactivation, very little fluorescence at 488-nm excitation was seen in cells expressing PA-GFP (Fig. 3A). This contrasted with cells expressing WEGFP, which exhibited significant fluorescence at 488-nm excitation before photoactivation (Fig. 3A). Upon photoactivation with 413-nm laser light (Fig. 3A) or with a 100 W Hg^{2+} lamp (fig. S4), fluorescence increases of >60-fold (figs. S3 and S4) were observed under 488-nm excitation in PA-GFP–expressing cells, whereas a fluorescence increase of only ~2.6-fold was observed in WEGFP-expressing cells (Fig. 3A and fig. S3). After photoactivation, both PA-GFP and WEGFP exhibited comparable levels of 488-nm fluorescence (Fig. 3A); therefore, the superior optical contrast of PA-GFP is due to its absence of significant 488-nm excited fluorescence before photoactivation.

To determine whether PA-GFP photoactivation could be used as a tool for measuring protein dynamics within living cells, we selectively photoactivated a subpopulation of PA-GFP molecules in expressing cells and observed their behavior over time (Fig. 3, B and C). Under low levels of 413-nm excitation (Fig. 3B), PA-GFP was distributed uniformly throughout the cell and showed virtually no fluorescence under 488-nm excitation. After ~1 s of photoactivation with high levels of 413-nm light within the region outlined in red (corresponding to the nucleus as determined by Nomarski imaging), the nuclear pool of PA-GFP became highly fluorescent under 488-nm excitation (Fig. 3B). Continued imaging with 488-nm light revealed rapid movement of the photoactivated molecules across the nuclear envelope and into the cytoplasm, resulting in their equilibration throughout the cell in a matter of minutes (Fig. 3, B and C, and movie S1). A similar rapid equilibration of fluorescent PA-GFP molecules between cytoplasm and nucleus was observed when the cytoplasm was photoactivated (movie S2). Thus, photoactivation of PA-GFP can be used to rapidly mark a selected population of molecules within cells and then to follow their kinetics over time.

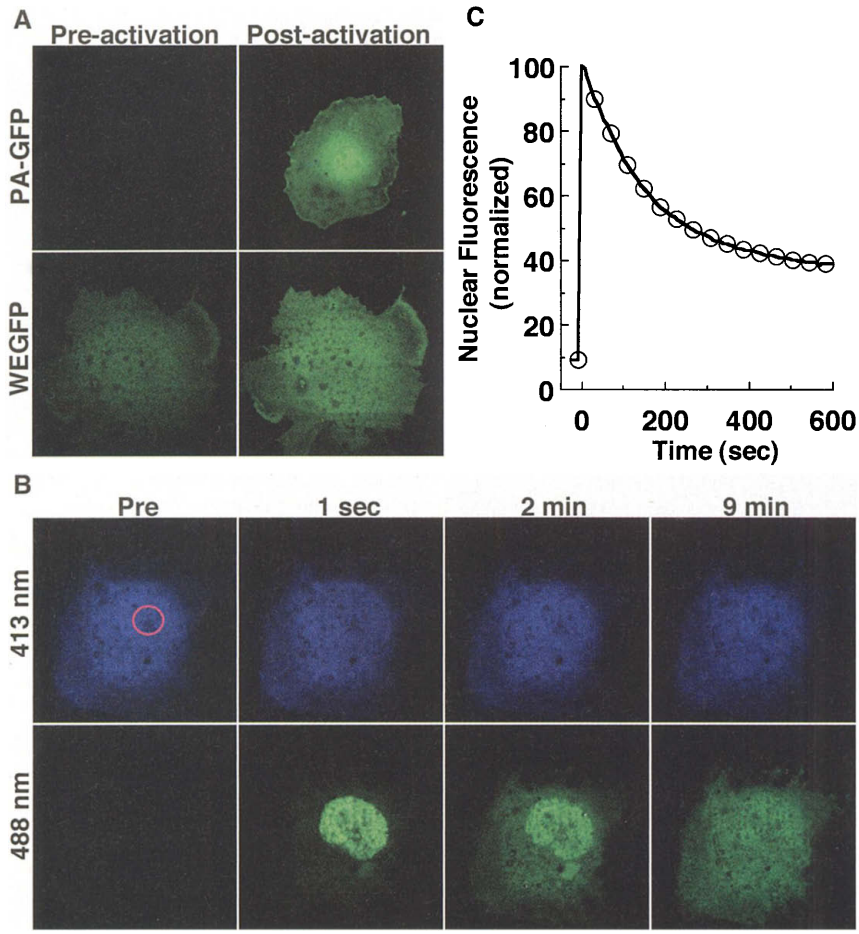

Fig. 3. Photoactivation and imaging in vivo. (**A**) PA-GFP and WEGFP were expressed in COS 7 cells and imaged with low levels of 488-nm laser light before (preactivation) and after (postactivation) irradiation of the field with high levels of 413-nm light. (**B**) A cell expressing PA-GFP was imaged with low levels of 413-nm excitation (blue images) and low levels of 488-nm excitation (green images) before (Pre), ~1 s, 2 min, and 9 min after photoactivation in the red region, which corresponds to the nucleus as determined by differential interference contrast imaging. (**C**) The nuclear level of PA-GFP fluorescence under low levels of 488-nm excitation was monitored before and after photoactivation within the nucleus.

In the above experiment, only photoactivated PA-GFP molecules exhibit noticeable fluorescence. Because of this, there is no concern that newly synthesized molecules will become fluorescent and complicate the results, which can occur when studying protein dynamics by photobleaching methods (*15*). Furthermore, photoactivation of PA-GFP could produce a population of highlighted proteins more rapidly and with greater optical enhancement than selectively photobleaching outside a similar population of EGFP molecules (*9*). The rapid and sizable optical enhancement obtainable by using PA-GFP photoactivation, therefore, makes it uniquely suited for analyzing protein kinetics within cells.

The utility of PA-GFP photoactivation for addressing biological questions was demonstrated in experiments that revealed new features of interlysosome protein exchange. Lysosomes receive and digest endocytic cargo by using hydrolytic enzymes (*16*). As such, they are considered to be terminal organelles with limited exchange of their membrane components [but see (*17*)]. To investigate the extent that membrane components exchange between lysosomes, we attached PA-GFP to the COOH-terminus of the lysosomal membrane protein, lgp120 (*18*, *19*) (PA-GFP–lgp120) and expressed it in cells. Addition of the PA-GFP tag near the COOH-terminal lysosomal sorting signal of lgp120 had no apparent effect on the ability of the chimera to target to lysosomes, because at steady state it colocalized with the lysosome-associated membrane protein-2 (Lamp-2) (Fig. 4, A to C). In cells expressing PA-GFP–lgp120 loaded with rhodamine-labeled albumin (red structures in Fig. 4, E, H, and K) as a lysosome cargo marker, little fluorescence was seen under 488-nm excitation (green) before photoactivation (Fig. 4D). After

~1 s of intense 413-nm irradiation of a small central region of the cell (see red box, Fig. 4D), bright fluorescent lysosomes were seen in this region under 488-nm excitation. Initially, the photoactivated signal was limited to the area inside the box, but within 10 s (Fig. 4G), the signal could be found in lysosomes outside this area. By 20 min (Fig. 4J), the majority of all lysosomes contained the photoactivated PA-GFP–lgp120 (movie S3). Counting the structures containing rhodamine-albumin revealed that 28% of lysosomes contained the photoactivated protein at 10 s after photoactivation compared with 74% at 20 min, indicating surprisingly extensive movement of PA-GFP–lgp120 between lysosomes. Disruption of microtubules with nocodazole treatment dramatically inhibited the lysosome exchange of photoactivated PA-GFP–lgp120 (Fig. 4, M to O; movie S4), indicating that movement of PA-GFP–lgp120 between lysosomes depends on the existence of an intact microtubule network. These findings

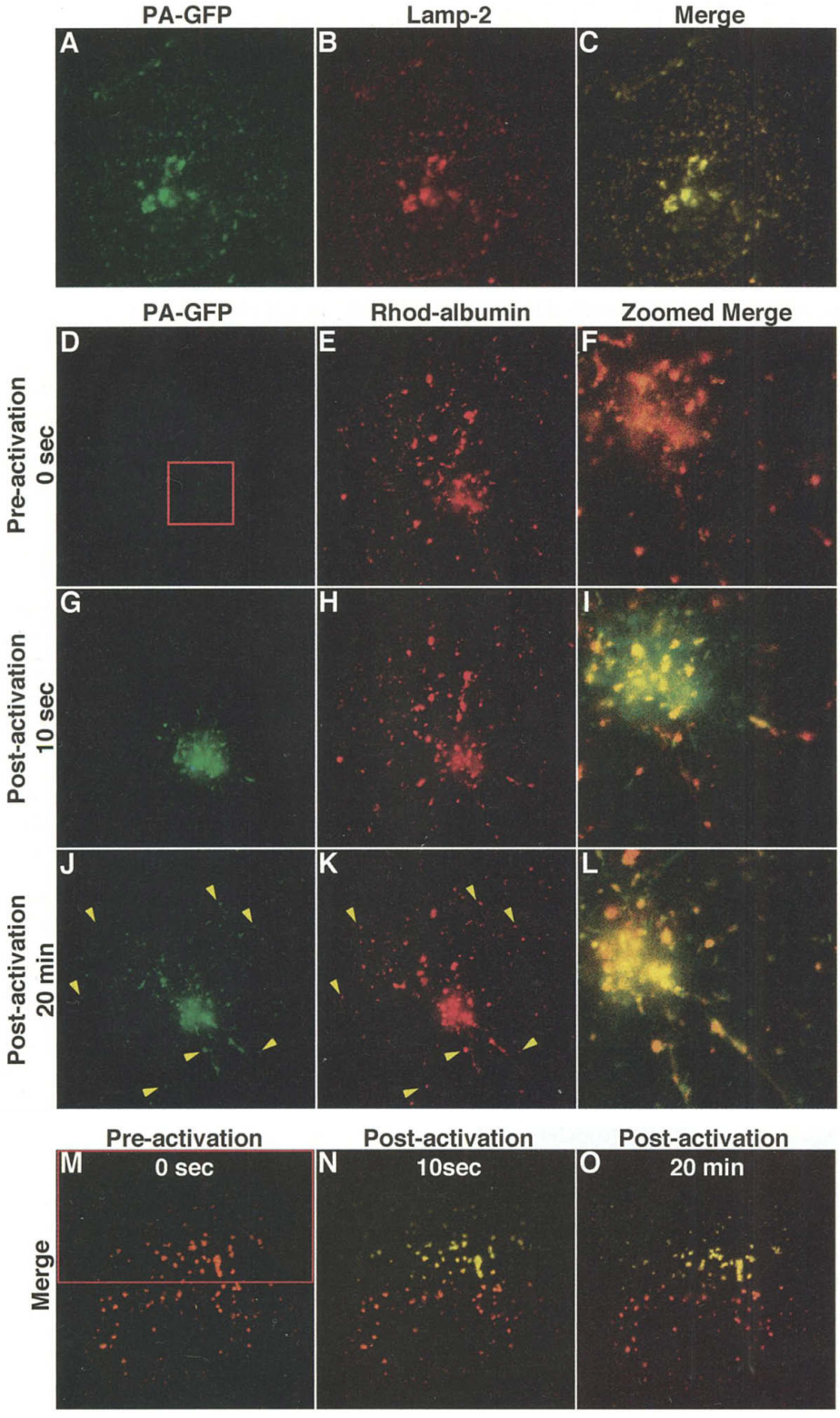

Fig. 4. Photoactivation of PA-GFP–lgp120 in COS 7 cells. (**A** to **C**) Cells were fixed and immunostained for the lysosomal membrane protein, Lamp-2. The entire cell was photoactivated and PA-GFP–lgp120 imaged under 488-nm excitation (A); the immunostained Lamp-2 was imaged under 543-nm excitation (B). When the two images are merged (**C**), colocalization of PA-GFP–lgp120 with Lamp-2 is seen. (**D** to **L**) A cell expressing PA-GFP–lgp120 was loaded with rhodamine-labeled albumin as a lysosome cargo marker. The markers were imaged by using 488-nm excitation (green images; D, G, and J) and 543-nm excitation (red images; E, H, and K), respectively, at time points before (D, E, and F; preactivation), ~10 s (G, H, and I; postactivation), and 20 min (J, K, and L; postactivation) after photoactivation of the regions indicated in the red square (D). The merged images (F, I, and L) show an enlarged view of the central region at the indicated time points. (**M** to **O**) Cells expressing PA-GFP–lgp120 and loaded with rhodamine-labeled albumin were incubated on ice for 15 min in the presence of 5 μg/ml nocodazole. Merged images shown before (M; preactivation), ~10 s (N; postactivation), and 20 min (O; postactivation) after photoactivation of the region indicated in red. Note the 10-s delay between photoactivation and the next image. Photoactivation was rapid, ~1 s for the region indicated in (D) and ~4 s for the region indicated in (M). The necessity of switching between different dichroic mirrors required for photoactivation and simultaneous imaging of GFP and rhodamine resulted in the ~10-s delay. Quantification of exchange was determined by counting the rhodamine-albumin positive structures that also contained photoactivated PA-GFP–lgp120.

confirm the existence of an exchange pathway between lysosomes (*17*, *20*) and indicate that such movement occurs with rapid kinetics by a microtubule-dependent mechanism.

In summary, we have described a photoactivatable variant of GFP, PA-GFP, that provides a powerful tool for investigating fundamental questions in cell and developmental biology. Upon photoactivation, PA-GFP exhibits an optical enhancement of nearly two orders of magnitude under aerobic conditions, making it suitable to mark specific protein or cell populations. The speed with which an optical signal is obtained and the absence of signal from newly synthesized proteins, furthermore, make PA-GFP photoactivation a preferable labeling method to photobleaching for studying the temporal and spatial dynamics of proteins in vivo.

References and Notes

1. J. C. Politz, *Trends Cell Biol.* **9**, 284 (1999).
2. H. Yokoe, T. Meyer, *Nature Biotechnol.* **14**, 1252 (1996).
3. M. B. Elowitz, M. G. Surette, P.-E. Wolf, J. Stock, S. Leibler, *Curr. Biol.* **7**, 809 (1997).
4. K. E. Sawin, P. Nurse, *Curr. Biol.* **7**, R606 (1997).
5. J. S. Marchant, G. E. Stutzmann, M. A. Leissring, F. M. LaFerla, I. Parker, *Nature Biotechnol.* **19**, 645 (2001).
6. M. Chalfie, Y. Tu, G. Euskirchen, W. W. Ward, D. C. Prasher, *Science* **263**, 802 (1994).
7. R. Y. Tsien, *Annu. Rev. Biochem.* **67**, 509 (1998).
8. Materials and methods are available as supporting material on *Science* Online.
9. Supporting text is also available on *Science* online.
10. K. Brejc *et al.*, *Proc. Natl Acad. Sci. U.S.A.* **94**, 2306 (1997).
11. G. J. Palm *et al.*, *Nature Struct. Biol.* **4**, 361 (1997).
12. J. J. van Thor, T. Gensch, K. J. Hellingwerf, L. N. Johnson, *Nature Struct. Biol.* **9**, 37 (2002).
13. R. Heim, D. C. Prasher, R. Y. Tsien, *Proc. Natl. Acad. Sci. U.S.A.* **91**, 12501 (1994).
14. T. Ehrig, D. J. O'Kane, F. G. Prendergast, *FEBS Lett.* **367**, 163 (1995).
15. J. Lippincott-Schwartz, E. Snapp, A. Kenworthy, *Nature Rev. Mol. Cell Biol.* **2**, 444 (2001).
16. S. Kornfield, I. Mellman, *Annu. Rev. Cell Dev. Biol.* **5**, 483 (1989).
17. Y. Deng, B. Storrie, *Proc. Natl Acad. Sci. U.S.A.* **85**, 3860 (1988).
18. V. Lewis *et al.*, *J. Cell Biol.* **100**, 1839 (1985).
19. C. L. Howe *et al.*, *Proc. Natl. Acad. Sci. U.S.A.* **85**, 7577 (1988).
20. A. L. Ferris, J. C. Brown, R. D. Park, B. Storrie, *J. Cell Biol.* **105**, 2703 (1987).

21. We thank D. Piston (Vanderbilt University) for the pRSETA-wtGFP and pRSETA-EGFP plasmids and I. Mellman (Yale University) for the lgp120 cDNA. The monoclonal antibody, H4B4, developed by J. T. August and J. E. K. Hildreth was obtained from the Developmental Studies Hybridoma Bank developed under the auspices of the NICHD and maintained by the Department of Biological Sciences, the University of Iowa, Iowa City, IA 52242. We also thank N. Altan-Bonnet, I. Arias, J. Bonifacino, D. Hailey, K. Hirschberg, J. Hurley, C. Jackson, A. Pfeifer, E. Snapp, and T. Ward for critical readings of this manuscript. G.P. was an Intramural Research Training Award fellow during this work.

Supporting Online Material

www.sciencemag.org/cgi/content/full/297/5588/1873/DC1
Materials and Methods
Supporting Text
Figs. S1 to S4
Tables S1 and S2
Movies S1 to S4

11 June 2002; accepted 5 August 2002

Observation of a Membrane Fusion Intermediate Structure

Lin Yang[1] and Huey W. Huang[2]*

We report the observation of a phase of phospholipid that contains a structure similar to the commonly postulated interbilayer state that is crucial to membrane fusion. The widely accepted model for membrane fusion suggests that there is an intermediate state in which the two contacting monolayers become continuous via an hourglass-shaped structure called a stalk. Many efforts have been made to estimate the free energy for such a state in order to understand the functionality of membrane fusion proteins and to define key parameters in energy estimates. The observation of the stalk structure supports the stalk hypothesis for membrane fusion and enables the measurement of these parameters experimentally.

Membrane fusion takes place during many cellular processes, including membrane traffic, fertilization, and infection by enveloped viruses. Fusion allows the exchange of contents between different membrane compartments. In order to maintain the individuality of each of the intracellular compartments and of the cell itself, membranes do not fuse easily under normal circumstances. Thus, the process requires special proteins and is subject to selective control. Understanding the fusion mechanism is important not only for fundamental biology but also for medical applications such as drug delivery and gene therapy. Substantial progress has been made in the elucidation of the structures of membrane fusion proteins (*1*, *2*) and in the estimations of the free energies for the rearrangement of lipid bilayers during fusion (*3*–*8*). Theoretical studies have identified the free energy barriers that suggest a requirement for mechanical work by fusion proteins, providing guidance for identifying the functions of protein structures. However, how proteins induce membrane fusion remains speculative, even in the best-studied case of viral fusion proteins (*1*, *9*–*13*), because key intermediate structures have not been observed.

Membrane fusion between phospholipid bilayers can be induced by a variety of chemicals (*14*), perhaps most simply by multivalent ions (*15*, *16*). The apparent role of multivalent ions is to bring two apposing lipid bilayers into contact. Here, we directly dehydrated the water layer between bilayers to achieve the same purpose. We started with a lipid spread on a flat substrate and exposed it to high humidity. Equilibrated under such conditions, the lipid formed a stack of parallel bilayers equally spaced by water layers (*17*). When hydration was reduced, point contacts between bilayers occurred and the two apposed monolayers merged at the contact point and developed into an hourglass-like interbilayer structure (Fig. 1A) called a stalk (*18*, *19*). This process is very likely analogous to the initial steps of membrane fusion. The difference here is that stalk structures were developed at numerous points of interbilayer contacts throughout the stack of bilayers. The system minimized energy by arranging the stalk structures into a regular lattice as in crystallization. This arrangement allowed us to inspect the stalk structure by x-ray diffraction.

One important characteristic of a lipid molecule is the ratio of the cross sections between its hydrophilic headgroup and its hydrocarbon chains. If this ratio is smaller than one, the lipid monolayer would have a tendency to bend toward the side of the headgroup. This is defined as a negative spontaneous curvature. It is well known that lipids with such a propensity tend to promote membrane fusion (*20*). We used diphytanoyl phosphatidylcholine (DPhPC), a lipid that has a negative spontaneous curvature. When DPhPC from organic solvent was deposited on a clean, flat substrate, it formed multiple parallel bilayers if the sample was kept warm ($> 20°C$) and in contact with saturated water vapor (*21*). To perform x-ray diffraction, we chose for the substrate a silicon nitride window (100 nm thick) spanned over a silicon frame, so that both transmissive and reflective diffraction could be recorded. Within the range of 20° to 30°C and relative humidity (RH) of 50 to 100%, three distinct diffraction patterns appeared (Fig. 1, B to E). Above ~80% RH, the lipid was in a lamellar (L_α) phase. The electron density profiles constructed from the diffraction patterns (Fig. 1C) showed that lipid bilayers, each ~3.8 nm in thickness, formed parallel lamella, intercalated with ~1-nm-thick water layers (*22*). When the relative humidity was decreased to between ~70 and ~80%, a different phase of phospholipid was discovered. The diffraction

[1]National Synchrotron Light Source, Brookhaven National Laboratory, Upton, NY 11973, USA. [2]Department of Physics and Astronomy, Rice University, Houston, TX 77251, USA.

*To whom correspondence should be addressed. E-mail: hwhuang@rice.edu